

1
2
3
4
5
6
7
8
9
10
11
12
13
14
15
16
17
18
19
20
21
22
23
24
25
26
27
28
29
30
31
32

Dissolved organic carbon dynamics in the East China Sea and the northwest Pacific Ocean

Ling Ding¹, Tiantian Ge¹ and Xuchen Wang^{1,2,*}

¹ Key Laboratory of Marine Chemistry Theory and Technology, Ministry of Education; Institute of Ocean Studies, Ocean University of China, Qingdao, 266100, China

² Center for Isotope Geochemistry and Geochronology, Qingdao National Laboratory for Marine Science and Technology, Qingdao, 266061, China

*Correspondence: Xuchen Wang (xuchenwang@ouc.edu.cn)

Keyword: Ocean carbon cycle, Dissolved organic carbon, East China Sea, North Pacific Ocean, Ocean water mixing

33 **Abstract.** Oceanic dissolved organic carbon (DOC) represents one of the largest carbon
34 reservoirs on Earth, and its distribution and biogeochemical cycles play important roles in
35 carbon cycling and other biogeochemical processes in the ocean. We report the distribution and
36 concentrations of DOC for water samples collected from the shelf-edge and slope regions in
37 the East China Sea (ECS) and the Kuroshio Extension (KE) in the northwestern North Pacific
38 during two cruises in 2014-2015. The DOC concentrations were 45-88 μM in the ECS and 35-
39 65 μM in the KE. In addition to biological processes that are estimated to account for 7% and
40 8-20% in shaping the DOC distribution in the ECS and KE regions, respectively, the DOC
41 distribution is largely controlled by hydrodynamic mixing of different water masses. By
42 comparing the DOC results with dissolved inorganic carbon (DIC) and dissolved inorganic
43 radiocarbon ($\Delta^{14}\text{C}$ -DIC) measured from the same water samples, we further demonstrate that
44 the intrusion of the Kuroshio Current could dilute the DOC concentrations at stations in the
45 outer shelf and slope regions of the ECS. The concentrations of DOC in the KE were
46 significantly lower in surface waters than in the ECS, and a relatively low and stable DOC level
47 ($\sim 40 \mu\text{M}$) was found in deep water (below 1500 m) at all stations. Based on the previously
48 reported DIC and $\Delta^{14}\text{C}$ -DIC values for the stations, the observed spatial variations of DOC in
49 the upper 700 m among the stations in the KE were mainly influenced by mixing of the two
50 water masses carried by the Kuroshio and Oyashio, the two dominant western boundary
51 currents in the region. The hydrodynamic processes are thus important factors in the distribution
52 and dynamics of DOC in the KE region.

53

54

55

56

57

58 **1 Introduction**

59 The world's oceans contain the second largest reservoir of carbon on earth, and dissolved
60 organic carbon (DOC) is the largest reduced carbon pool (685 Pg C) in the ocean (Hansell and
61 Carlson, 1998; Hansell et al., 2009). The DOC in the ocean consists of a highly diverse organic
62 molecular mixture in which ~20,000 individual molecular formulae have been detected (Riedel
63 and Dittmar, 2014). The concentration and distribution of ocean DOC play significant roles not
64 only in the global carbon cycle but also in control and regulation of the microbial community
65 and many biogeochemical processes in the oceans (Azam et al., 1983; Fenchel, 2008; Carlson
66 et al., 2010; Nelson and Carlson, 2012). Because ocean DOC is directly linked to the oceanic
67 dissolved inorganic carbon (DIC) system through biological photosynthesis and microbial
68 respiration processes, the DOC pool in the ocean also indirectly contributes to the cycles of
69 atmospheric CO₂ (Druffel et al., 1992; Carlson et al., 1994; Carlson et al., 1998; Hansell and
70 Carlson, 2001; Carlson et al., 2010).

71 In the most recent 20 years, improved precision of DOC concentration analysis via the high-
72 temperature catalytic oxidation (HTCO) technique has revealed detailed oceanic DOC
73 distributions, such as those generated by the US Climate Variability Repeat (CLIVAR)
74 hydrography program (Sharp et al., 1995; Sharp et al., 2002; Carlson et al., 2010; Hansell et al.,
75 2012; Bercovici and Hansell, 2016). In general, biological and physical processes combine in
76 modulating the distribution and dynamics of DOC in open oceans (Hansell and Waterhouse,
77 1997; Ogawa et al., 1999; Hansell et al., 2009; Carlson et al., 2010; Bercovici and Hansell,
78 2016). It has been widely observed that oceanic DOC accumulates in the upper water column
79 (100 m) at elevated concentrations (70-90 μM) compared with its relatively constant values
80 (35-45 μM) in deep water (>1000 m), reflecting biological production of DOC in the euphotic
81 zone and microbial consumption with depth (Hansell et al., 2009). However, many previous
82 studies conducted in different coastal and open oceans have shown that the distribution of DOC

83 appeared to depend, to a large extent, on the hydrographical structure and/or horizontal/ vertical
84 water mixing (Hansell and Waterhouse, 1997; Hansell and Peltzer, 1998; Hung et al., 2007;
85 Ogawa et al., 2003; Guo et al., 1995) and the secondary biological forcing superimposed on the
86 physical forcing (Carlson et al., 2010; Wu et al., 2017). Based on a water mixing model, Wu et
87 al. (2017) also reported that microbial degradation contributed 10% of the DOC removal and
88 that physical mixing controlled the majority variation of the DOC pool in the northern South
89 China Sea.

90 The northwestern North Pacific is a rather special oceanic region where carbon cycling and
91 biogeochemical processes are greatly influenced by two major oceanic western boundary
92 currents: the Kuroshio Current (KC) and Oyashio Current (OC). As one of the largest
93 marginal sea in the northwestern North Pacific, the hydrological characteristics of the East
94 China Sea (ECS) are largely influenced by vigorous exchange between the warm saline
95 Kuroshio and cold fresh continental shelf water masses (Hsueh, 2000). Ogawa et al. (2003)
96 reported that the distribution of DOC was primarily controlled by hydrological rather than by
97 biological processes around the shelf edge of the ECS. However, few studies have focused on
98 the distribution and dynamics of DOC around the Kuroshio Extension region. DOC ^{14}C analysis
99 from different North Pacific stations revealed the export of young DOC accompanied by the
100 North Pacific Intermediate Water (NPIW) formation, resulting in an enrichment in the $\Delta^{14}\text{C}$ -
101 DOC values and a reduction in the notably old DOC ^{14}C -age in the Pacific Ocean interior
102 (Druffel et al., 1992; Druffel et al., 2019), but the vertical profiles of DOC were only determined
103 at stations in the subpolar water in the northwestern North Pacific (Hansell et al., 2002). DOC
104 observations in the WOCE (World Ocean Circulation Experiment) and CLIVAR cruises were
105 collected at Line P02 stations along a 30°N latitudinal transect, but the distribution of DOC
106 near the KE was not investigated during these cruises.

107 Overall, our understanding of DOC dynamics and cycling in the outer shelf and slope regions

108 of the ECS and KE region is still limited. In this work, we present the results from DOC
109 concentrations measured in the ECS and KE region in the northwestern North Pacific combined
110 with the observations of dissolved inorganic carbon (DIC) concentrations and dissolved
111 inorganic radiocarbon ($\Delta^{14}\text{C}$ -DIC) values for an evaluation of the roles of the physical mixing
112 process on the distribution of DOC in these two different dynamic oceanic regions.

113 **2 Methods**

114 **2.1 Study areas**

115 Water samples were collected from two main oceanic regions: the ECS and the KE region in
116 the northwestern North Pacific (Fig. 1). The ECS is one of the largest marginal seas connected
117 to the northwest North Pacific, with a broad continental shelf area of approximately 0.5×10^6
118 km^2 (Gong et al., 2003). In the relatively shallow (<60 m) and wider inner shelf region, oceanic
119 processes are largely influenced by the inputs of the Yangtze and Yellow Rivers, which are the
120 largest and second largest rivers in China, and each delivers 1.58×10^{12} g DOC and 3.20×10^{10} g
121 DOC into the ECS (Wang et al., 2012; Xu et al., 2016). In the outer shelf and slope region of
122 the ECS, the hydrographic characteristics and oceanic processes are affected largely by the
123 northward-flowing Kuroshio Current, which impinges on the shelf break; and a branch of the
124 Kuroshio Current enters the ECS across the shelf break (Chen and Wang, 1999; Guo et al., 2006;
125 Hu et al., 2015; Ge et al., 2016). The high primary productivity and intersection of different
126 water masses make the ECS a complex region for studying the ocean carbon biogeochemical
127 cycle.

128 The Kuroshio Extension (KE) in the northwestern North Pacific is an important and highly
129 dynamic region that is largely influenced by the Kuroshio and Oyashio currents. The Kuroshio
130 Current carrying relatively warm and saline waters flows northward along the east coast of
131 Japan, turns eastward near $34^\circ \text{N}/140^\circ \text{E}$, and subsequently flows as the KE into the North

132 Central Pacific (Yasuda et al., 1996; Qiu, 2001; Qiu and Chen, 2011). The southward-flowing
 133 Oyashio Current, which carries fresh and cold subarctic water, meets with Kuroshio water at
 134 approximately 37 °N and forms the Kuroshio-Oyashio inter-frontal zone where the subarctic
 135 water mass mixes with the KE water and flows eastward (Yasuda et al., 1996; Qiu and Chen,
 136 2011; Hu et al., 2015). The new NPIW is formed in the same region and is a mixture of relatively
 137 fresh and recently ventilated Oyashio water and high-salinity Kuroshio water (Yasuda et al.,
 138 1996; Talley, 1997; Qiu and Chen, 2011). The mixed water region in the KE has been
 139 characterized as an important sink of anthropogenic CO₂ in the northwestern North Pacific
 140 (Tsunogai et al., 1993), and it is a key area for understanding regional climate and ecosystem
 141 variations and biogeochemical cycles (Yasuda, 2003; Wu et al., 2012; Hu et al., 2015; Nishibe
 142 et al., 2017).

143

144 **Table 1.** Summary of sampling stations and times in the East China Sea (ECS) and the Kuroshio
 145 Extension (KE) in the northwestern North Pacific (NP).

Station #	Latitude (°N)	Longitude (°E)	Water depth (m)	Sampling Date
<u>ECS</u>				
Stn.1	28.37	126.69	177	12 July 2014
Stn.7	28.30	126.83	265	12 July 2014
Stn.11	28.43	126.53	148	13 July 2014
Z1	28.07	127.13	1078	14 July 2014
Z2	27.93	127.36	1326	14 July 2014
Z4	28.63	127.00	425	14 July 2014
Z3	27.75	126.63	1415	15 July 2014
<u>KE in NP</u>				
K2	25.10	134.02	4100	5 April 2015
B2	37.00	147.00	5586	27 April 2015
B8	30.97	146.99	6000	11-12 April 2015
B9	29.86	146.53	5500	10-11 April 2015
A1-b	32.63	145.95	4800	18 April 2015
A4	34.00	147.80	5800	25 April 2015
A6	34.02	150.04	5800	23 April 2015
A8	34.04	152.02	5500	21 April 2015

146

147 **2.2 Sample collection**

148 Water samples for DOC analysis were collected from 7 stations on the shelf-edge and slope
149 region of the ECS during a cruise in July 2014 onboard the Japanese *R/V Shinset Maru* and
150 from 8 deep stations in the KE region and western North Pacific during a cruise in April-May
151 2015 onboard the Chinese *R/V Dongfanghong-2* (Fig. 1). General information on the sampling
152 stations is summarized in Table 1. All water samples were collected using 12 L Niskin bottles
153 deployed on a rosette with a calibrated SeaBird CTD (model SBE 911) that recorded the
154 temperature and salinity profiles. The accuracies for temperature and salinity are 0.001 °C and
155 0.001, respectively.

156 After collection, water samples from the Niskin bottles were transferred directly into a 1 L
157 pre-combusted (at 550 °C for 4 h) glass bottle after rinsing three times with seawater. The water
158 was filtered immediately on board through Whatman GF/F filters with 0.7 µM pore size
159 (prebaked at 550 °C for 4 h). The filtered water samples were acidified with super-high-purity
160 85% H₃PO₄ (Aladdin[®]) to pH = 2 and preserved in a frozen state at -20 °C until chemical analysis.

161 **2.3 Chemical analysis**

162 Concentrations of DOC were analysed by the high temperature catalytic oxidation (HTCO)
163 method (Sharp et al., 1995; Sharp et al., 2002) using a Shimadzu TOC-L analyser equipped
164 with an ASI-V autosampler. Potassium hydrogen phthalate (KHP) dissolved in high-purity
165 Milli-Q water was used as the DOC standard. The quality assessment for DOC measurements
166 was checked against reference low-carbon water and deep-sea water which were analysed every
167 10 samples (CRM Batch 13 with 41-44 µM DOC concentration, supplied by Hansell
168 Biogeochemical Laboratory at University of Miami, USA). The average value and standard
169 deviation of deep-sea water reference throughout our measuring was 43 ± 1 µM, which was used
170 as an index of our analytical precision. The instrumental blank was subtracted using high-purity
171 Milli-Q water that was analysed between samples (before every sample for deep seawater). The

172 average blank of the DOC measurement was $\leq 5 \mu\text{M}$, and the analytical precision on triplicate
173 injections were $\pm 3\%$. All samples were analysed in duplicate from different vials, and the
174 average values were reported. The standard deviation for DOC ranged in $\pm 0.1- 4.0 \mu\text{M}$.

175 The methods for DIC concentrations and $\Delta^{14}\text{C}$ -DIC measurements were described in detail
176 in separate papers for the samples collected during the same cruises (Ge et al., 2016; Ding et
177 al., 2018). In brief, DIC concentrations were measured using a Shimadzu TOC-L analyser with
178 the total IC mode. Sodium carbonate and sodium bicarbonate dissolved in Milli-Q water were
179 used as the DIC standards, and the concentration values were checked against DIC reference
180 materials (deep sea water) for quality assessment (supplied by Dr Dickson at Scripps Institution
181 of Oceanography). The total blanks were approximately $< 0.15\%$ of the seawater DIC
182 concentrations, and the analytic precisions were $< 3\%$. For ^{14}C -DIC measurement, DIC was
183 first extracted as gaseous CO_2 using our modified method with extraction efficiencies $> 96\%$
184 (Ge et al., 2016). The ^{14}C -DIC values were analysed in the National Ocean Sciences Accelerator
185 Mass Spectrometry (NOSAMS) facility at Woods Hole Oceanographic Institution (WHOI).
186 The purified CO_2 was graphed for $\Delta^{14}\text{C}$ analysis using AMS. The $\Delta^{14}\text{C}$ values are reported as
187 the modern fraction based on the reference material used (McNichol et al., 1994). The
188 conventional ^{14}C ages (years before present or yr BP) were calculated following the method of
189 Stuiver and Polach (1977). The maximum total uncertainty is 6% , as tested with a DIC standard
190 (Ge et al., 2016).

191 **3 Results**

192 **3.1 Hydrography**

193 The hydrographic parameters of the sampling stations (temperature and salinity) recorded
194 with the CTD are summarized in Table S1 in the Supporting information, and the depth profiles
195 are plotted in Fig. S1. The hydrology of the water is further described in the T-S diagrams, as

196 plotted in Fig. 2. The physical properties of different water masses in the two oceanic regions
197 were extracted from literature and corresponded to the temperature and salinity of the water
198 types in their formation area or the values around the boundaries, which is also included in Fig.
199 2. Because our study involved two distinctive oceanic regions, we separately plotted the
200 hydrographic characters (T-S diagrams) for stations in the ECS (Fig. 2a) and KE (Fig. 2b)
201 regions.

202 As shown in Fig. 2a and Fig. S1 for the seven shelf-edge and slope stations in the ECS, the
203 water temperature was higher (26.3-29.3 °C) at the surface (≤ 10 m and $\sigma_t \leq 22.1$) and decreased
204 rapidly with depth at all stations. The salinity ranged from 33.88 to 34.87 and exhibited a
205 reversed S-shape, i.e., lower at the surface, increasing with depth to the maximum at 150 m
206 water depth (23.2-24.9 σ_t), and decreasing again to 500 m (26.4-26.8 σ_t). The salinity (S)
207 remained relatively constant below 500 m depth (at $\sigma_t > 26.8$) for the three slope stations (Fig.
208 2a and Fig. S1).

209 For Sta. K2 and the seven deep stations in the KE, the temperature (T) of the surface water
210 ranged from 14.7 to 24.4 °C, exhibited a rapid decrease and subsequently remained constant for
211 all stations at density levels of $\sigma_t > 27.6$ at ~1500 m depth (Fig. 2b and Fig. S1). The largest
212 temperature variations occurred in the upper 700 m with the highest T (24.4 °C) observed at Sta
213 K2 (end-member value of T in the Kuroshio water) and the lowest T (14.7 °C) at Sta B2 observed
214 in the surface layer (5 m) (end-member value of T in the Oyashio water) (Fig. 2b). The salinity
215 (S) for these stations was higher at the surface, decreased initially to reach a minimum at the
216 density range of 26.4-26.9 σ_t , and subsequently increased with depth to approximately 2500 m
217 with the density layer of 27.6 σ_t (Fig. 2b). The salinity for all stations remained relatively
218 uniform below 2500 m ($\sigma_t > 27.6$). Similar to T , the largest differences in salinity also appeared
219 in the upper 700 m water column (the density range of 26.4-27.0 σ_t), where low salinity (34.49)
220 was observed at the surface of Sta B2. The salinity decreased to 33.66 near 250 m and

221 subsequently increased to values similar to those of the other stations at 2500 m. The salinity
222 for the remaining seven stations (Stas. K2, A1-b, A4, A6, A8, B8 and B9) showed less variation
223 in the surface layers (5 m) (34.76 to 34.98), and Sta K2 had the highest S (34.98) at the surface
224 among all stations (Fig. 2b and Fig. S1) (the typical salinity of Kuroshio water is 34.98 and
225 33.66 for the Oyashio water).

226 **3.2 Concentrations and distribution of DOC**

227 To examine the distribution of DOC with different water masses in the studied regions, we
228 plotted the depth profiles (Fig. 3) and the T-S-DOC diagrams for the ECS and the KE, as shown
229 in Fig. 4. The concentrations of DOC ranged from 45 to 88 μM in the ECS and from 35 to 65
230 μM in the KE region (Fig. 3 and Table S1). The concentrations of DOC ranged from 55 to 88
231 μM for the four shelf-edge stations (Stn. 11, 1, 7 and Z4) and from 45 to 84 μM for the three
232 slope stations (Stas. Z1, Z2 and Z3) in the ECS. As plotted in Fig. 3a and Fig. 4a, the
233 concentrations of DOC showed less variation (71-81 μM) in the surface water (≤ 10 m and $\sigma_t \leq$
234 22.1) and decreased rapidly to ~ 300 m depth for all stations in the ECS. Below 300 m, the
235 concentrations of DOC remained relatively constant down to 1000-1400 m depth for Z1, Z2
236 and Z3 (Fig. 3a).

237 The concentrations of DOC in the KE region were much lower than that in the ECS, and
238 above 1000 m the stations showed large spatial variations (Fig. 3b). The highest DOC value (65
239 μM) and the lowest DOC level (43 μM) were measured at the surface at Sta K2 and Sta B2,
240 respectively. In the upper 200 m depth, the concentrations of DOC also showed a notably rapid
241 decrease for most stations. The DOC concentrations were visibly lower at Sta A4 and Sta B2
242 (36-53 μM) than at the other stations in the upper 700 m depth (at $\sigma_t < 27.0$), whereas the
243 concentrations were slightly higher in the 500-800 m depth at Sta B8 and Sta A8. The T-S-DOC
244 diagrams showed that DOC concentrations decreased to relative low levels (36-44 μM) at all
245 stations at $\sigma_t > 27.5$ (approximately below 1500 m depth) and remained constant in deep waters

246 (Fig. 3b and Fig. 4b).

247 **3.3 Concentrations and radiocarbon distribution of DIC**

248 The results of the DIC concentrations and $\Delta^{14}\text{C}$ -DIC values measured from the same samples
249 have been recently published (Ge et al., 2016; Ding et al., 2018). In this work, we use these data
250 as water mass tracers to support our DOC results. In brief, as shown in Fig. 5a, the DIC
251 concentrations were higher in the four shelf-edge stations (Stn.11, Stn.1, Stn.7 and Z4) than that
252 in the slope stations (Z1 and Z2) at the same depths in the ECS (Fig. 5a). The depth profiles of
253 $\Delta^{14}\text{C}$ -DIC showed a trend opposite to that of the concentrations of DIC, i.e., higher at the
254 surface and decreasing with depth (Fig. 5b). Higher DIC concentrations had lower $\Delta^{14}\text{C}$ -DIC
255 values. The $\Delta^{14}\text{C}$ -DIC values at 138 m for Stn.11 and 413 m for Stn. Z4 were significantly
256 lower than the values of the slope stations at the same water depths (Fig. 5b).

257 The concentrations of DIC were also lower at the surface and increased with depth for the
258 stations in the KE region (Fig. 5c). The large variability in DIC concentrations was observed
259 between 400 and 800 m depths. The $\Delta^{14}\text{C}$ -DIC values were high at the surface, decreased with
260 depth and showed large variations in the upper 250-1000 m among the stations (Fig. 5d). The
261 $\Delta^{14}\text{C}$ -DIC values showed a rapid drop within only the upper 500 m of the water column at Sta
262 A4 and in the upper 1000 m depth at Sta B2 and subsequently remained constant below 1000
263 m depth. The $\Delta^{14}\text{C}$ -DIC profiles for stations K2, A8, and B9 exhibited a similar trend. The
264 surface bomb ^{14}C signal mixed well down to 600 m and subsequently decreased until 1500 m
265 (1000 m for K2) (Fig. 5d).

266 **4 Discussion**

267 **4.1 Processes that control the DOC distribution in the ECS**

268 In this study, the concentrations of DOC measured in the shelf-edge and slope waters are
269 comparable to the values reported previously for the ECS (Hung et al., 2003; Ogawa et al.,

270 2003; Gan et al., 2016). As one of the large river-influenced shallow (~60 m) marginal sea,
271 many factors could influence the distribution of DOC. The inputs of the Yangtze and Yellow
272 rivers play important roles affecting the carbon cycling in the ECS. In their study, Wang et al.
273 (2012) and Xue et al. (2017) reported that the Yangtze and Yellow rivers delivered 3.1×10^{12} g
274 and 7.26×10^{10} g terrestrial organic carbon, comprised 45-50% DOC input to the ECS in 2009
275 and 2015. These riverine DOC was derived mainly from pre-aged soil organic matter with ^{14}C
276 ages of around 1,000 years old (Wang et al., 2012; Xue et al., 2017). The observed higher DOC
277 concentrations in the upper layer of the ECS could be caused by the riverine refractory DOC
278 that was cycled in the water for long time and transported offshore. In addition, DOC
279 concentration in the shallow shelf region of the ECS could be influenced by relatively high
280 primary production, flux from sediment and bacterial degradation (Ogawa et al., 2003; Wang
281 et al., 2012; Gan et al., 2016). However, export of DOC from the shelf water to the slope
282 offshore could be limited because most of the bioavailable DOC had been respired in the shelf
283 waters (Bauer and Bianchi, 2011; Bauer et al., 2013; Ward et al., 2017). In the shelf edge and
284 slope region of the ECS, early studies by Hung et al. (2003) and Ogawa et al. (2003) reported
285 that the distribution of DOC was primarily controlled by physical processes rather than
286 production and/or microbial processes. In this respect we observed a statistically significant
287 positive correlation between DOC and water temperature ($R^2 = 0.82$, $p < 0.001$) for the stations
288 in the ECS (Fig. 6a). A similar pattern has also been found in other marginal seas of the North
289 Pacific (Hung et al., 2007; Dai et al., 2009). In our recent study, we reported that the
290 concentrations of DIC and $\Delta^{14}\text{C}$ -DIC in the ECS slope and the KE region showed conservative
291 behaviour and could be used as tracers of water mass movement and water parcel
292 homogenization as predicted by the solution mixing model (Ge et al., 2016; Ding et al., 2018).
293 As shown in Fig. 6b, the negative relationship between DOC and DIC ($R^2 = 0.73$, $p < 0.001$)
294 for the stations further suggests that physical processes (such as horizontal and vertical water

295 mixing) influenced the distribution and variation of DOC in the shelf break and slope region of
296 the ECS. However, since DOC is not conservative in the ocean, the observed strong correlation
297 between DOC and T could involve biological and microbial processes and possibly depth co-
298 variation. Using this DOC-T correlation alone, we are not able to draw conclusion that
299 physical mixing was the controlling factor influencing the distribution of DOC in the ECS.

300 Although the river inputs play an important role in the ECS, our sampling stations in the slop
301 region are unlikely affected directly by freshwater input from the Yangtze River, according to
302 the high salinity without any freshwater dilution signals in Fig. 2a and Fig. S1. The vertical
303 variations of DOC for the shelf-edge and slope stations, as shown in Fig. 3a, followed a typical
304 trend similar to the DOC depth profiles observed in open oceans, with higher levels of DOC in
305 the low-density upper waters and low levels of DOC in the high-density deep waters. Around
306 the shelf-edge of the ECS, the vigorous exchange between the warm saline Kuroshio and cold
307 fresh continental shelf water masses affect the hydrographical characteristics (Hsueh, 2000). As
308 shown in Fig. 2a, the salinity maximum at the density range of 23.2-24.9 σ_t (near 100-160 m)
309 is influenced largely by the northward-flowing Kuroshio Current. Physical models and
310 chemical tracers both supplied clear evidence of the intrusion of upwelled Kuroshio
311 intermediate water (500-800 m) into the ECS shelf region (Yang et al., 2011; Yang et al., 2012;
312 Ge et al., 2016). To further demonstrate the influence of different water mass mixing processes
313 on the hydrological properties, Figure 7 compared the latitudinal distributions of salinity,
314 DOC/DIC concentrations and $\Delta^{14}\text{C}$ -DIC for the seven stations in the ECS. The cross-section
315 salinity plot (Fig. 7a) showed that the water mass in the studied area was composed of mixed
316 Kuroshio and shelf waters. It appeared likely that the influences of Kuroshio intermediate water
317 (500-800 m) on the bottom water at station Z4 and Stn. 11 brought low concentrations of DOC,
318 high concentrations and low $\Delta^{14}\text{C}$ values of DIC (Fig. 7b-d). This intrusion of Kuroshio
319 intermediate water diluted the DOC at Stn. 11 and Z4. However, it appears that this upwelling

320 intrusion had almost no effect on the surface water (<100 m depth) for the shelf stations. The
321 intrusion of Kuroshio intermediate water could reflect a smaller-scale or eddy effect rather than
322 a large-scale influence beyond Stn. 11 and Z4 (Ge et al., 2016).

323 The calculation based on the $\Delta^{14}\text{C}$ -DIC mass balance showed that approximately 54-65% of
324 the bottom water in the shelf region of ECS originated from the intrusion of Kuroshio
325 intermediate water (Ge et al., 2016). As referred to the water mass analysis on the basis of the
326 assumed conservative variables (potential temperature and salinity) as the characteristics of
327 water type (Catal et al., 2015a and 2015b), if we use the same two end-member mixing model
328 (Ge et al., 2016) and the corresponding average DOC values for the shelf water (77 μM) and
329 Kuroshio water (52 μM), the conservative concentrations of DOC (referred as DOC^0) could be
330 calculated in the range of 61-64 μM , which is slightly higher but comparable to the observed
331 DOC values in the bottom waters at Stn. 11 and Z4 (56-61 μM). The negative values of ΔDOC
332 ($\text{measured DOC} - \text{DOC}^0$) could represent the biological consumption effects superimposed on
333 the water physical mixing processes around the shelf-edge and in the slope of ECS. Based on
334 the calculated ΔDOC and the field-measured DOC, we estimated that the bioavailable fraction
335 of DOC could account for approximately 7% of the total DOC pool in this region. The value is
336 comparable to the results (6.1% and 10% \pm 5%) previously reported for the Kuroshio Current
337 and the shelf-slope region of the South China Sea (Gan et al., 2016; Wu et al., 2017). Clearly,
338 biological processes had a significant influence on DOC but were not the dominant controlling
339 factor on the observed DOC distributions in the ECS.

340 **4.2 Processes that influence the DOC profiles in the Kuroshio Extension**

341 In general, the biological and physical processes could both affect the DOC profiles in open
342 oceans (Hansell and Waterhouse, 1997; Ogawa et al., 1999; Hansell et al., 2009; Carlson et al.,
343 2010; Bercovici and Hansell, 2016). Based on a correlation analysis of data collected over ten
344 years in the KE region, Nishikawa et al. (2011) presumed that the shoaling of mixed layer depth

345 could reduce the nutrient supply from deep layers, resulting in less productivity around the KE
346 region in the spring. Low primary production was also observed during the spring time on
347 previous cruises between 2008 and 2011 in the KE region attributed primarily to the low
348 concentration of nitrate and silicic acid (Nishibe et al., 2015). Moreover, notably low levels of
349 available dissolved nitrogen ($< 4 \mu\text{M}$) were observed in the region (unpublished data) during
350 the same cruise in spring (April-May 2015). The relatively lower surface DOC concentrations
351 (average $57 \pm 7 \mu\text{M}$) could be due to the low primary production during sampling in the spring
352 season. Despite the low DOC concentrations in the region, we observed the interesting feature
353 of relatively large spatial variations for DOC concentration among these stations, especially in
354 the upper 1500 m (Fig. 3b and Fig. 4b). For example, concentrations of DOC in the upper 100
355 m depth at Stas B2 and A4 located north of and around the KE were significantly lower (average
356 $43 \pm 5 \mu\text{M}$) than those of other stations and were close to the deep water values (ca. $36\text{-}44 \mu\text{M}$,
357 average $39 \pm 3 \mu\text{M}$), while elevated concentrations of surface DOC ($61\text{-}65 \mu\text{M}$) prevailed at Sta
358 K2 located far south of KE and the other five stations ($54\text{-}63 \mu\text{M}$, Stas A1-b, B8, B9, A6 and
359 A8), with values 28% higher than average. In the KE region, primary production is largely
360 affected by advection along the KE meander and differs among representative areas in spring,
361 i.e., high in the northern edge and around the KE axis ($483\text{-}630 \text{ mg C m}^{-2} \text{ day}^{-1}$), accompanied
362 by high chlorophyll *a* concentration and high column integrated chlorophyll *a* values ($35\text{-}44$
363 mg m^{-2}) in April (Nishibe et al., 2015). The relatively high primary production should result in
364 a high level of DOC in the stations located north and around the KE, but the measured DOC
365 concentrations were rather low at Stas B2 and A4. In addition, surface mooring data from the
366 NOAA Kuroshio Extension Observatory (KEO) indicated that physical processes dominate the
367 carbon input to the mixed layer at KEO (Fassbender et al., 2017). Therefore, we speculate that
368 the low DOC levels at Sta B2 and A4 were unlikely directly related to the primary production,
369 and instead, the observed large spatial variations were mainly modulated by the mixing

370 dynamics of different water masses rather than biological processes in the region.

371 Hydrodynamic mixing can be directly evaluated by comparing the DOC concentrations with
372 the variables of hydrographic properties. In Figs. 6c and 6d, we examined the correlations of
373 the DOC concentrations with water temperature and DIC concentrations in the KE region,
374 respectively. Overall, a positive relationship exists between the DOC concentrations and
375 temperature in the KE (Fig. 6c, $R^2 = 0.62$, $p < 0.001$), and a negative correlation exists between
376 the DOC and DIC concentrations (Fig. 6d, $R^2 = 0.51$, $p < 0.001$). Considering the relatively
377 conservative behaviour of DIC in the open ocean, it could be used as tracers of water mass
378 movement and water parcel homogenization as predicted by the solution mixing model in the
379 KE region (Ding et al., 2018). The observed correlations of DOC concentrations and
380 hydrographic variables could thus indicate the physical water mixing played important roles on
381 the DOC distribution in the KE region. To further examine the distribution of DOC with
382 different water masses in the KE region, we plotted the DOC and DIC concentrations and $\Delta^{14}\text{C}$ -
383 DIC values superimposed on the plots of potential temperature (θ) and salinity in Fig. 8. It can
384 be observed that the distributions of DOC, DIC and $\Delta^{14}\text{C}$ -DIC were clearly associated with
385 different water masses, as identified by the temperature, salinity and potential density (σ_0) in
386 the T-S diagrams (Fig. 8). The denser water mass C with density levels of 26.4-27.1 σ_0 near
387 500-800 m (Fig. 8) likely originated from the subarctic gyre, which had low temperature and
388 salinity and was transported by the south-flowing Oyashio Current along the western boundary
389 to the KE region. This water is subsequently mixed with the warm saline water mass transported
390 by the northeast-flowing Kuroshio Current (water mass A) corresponding to the six stations
391 (K2, A1-b, A6, A8, B8 and B9) in the south of KE axis.

392 Many results suggested that hydrodynamic processes, such as the deep water penetration by
393 vertical mixing, possibly affected the DOC concentrations within the surface waters in the high
394 latitude despite high primary production (Ogawa et al., 1999; Ogawa and Tanoue, 2003).

395 Considering the relatively lower temperature ($< 15\text{ }^{\circ}\text{C}$) and salinity (< 34.5) in the upper 700 m
396 (Fig. 2b and Fig. S1), Sta B2 was mainly affected by the intrusion of cold and fresh subarctic
397 water transported by the southward-flowing Oyashio, which also carried lower concentrations
398 of DOC. In contrast, despite the nutrient-depleted and low primary productivity in the
399 subtropical gyre, physical stability factors such as water column stratification could restrict the
400 vertical mixing of the surface and deep waters, which is beneficial for DOC accumulation in
401 the surface layer. The similar patterns of hydrographic properties and relatively higher DOC
402 levels in the upper 500 m at Sta K2 and other five stations (A1-b, B8, B9, A6 and A8) in the
403 KE region suggested that the Kuroshio water dominated the mixing in the upper 500 m at these
404 stations, which are mainly characterized with a subtropical warm and high-salinity water mass,
405 as demonstrated in Fig. 3b and Fig. S1. The regional influences of the two water masses carried
406 by Kuroshio and Oyashio currents can be demonstrated more clearly in Fig. 9, where we plotted
407 the salinity, DOC and DIC concentrations, and $\Delta^{14}\text{C-DIC}$ values for the five stations (B2, A4,
408 A1-b, B8 and B9) as a cross KE transect from north to south. It can be observed that the
409 Kuroshio, which carries relatively high DOC, dominated stations B9, B8 and A1-b above 500
410 m depth. The latitudinal distributions of salinity could serve as intuitive evidence to show the
411 intrusion of Oyashio Current, which resulted in the low salinity near 200-800 m at Sta B2 and
412 other two reference stations at the north and near of 35°N labelled in Fig. 9e (at a density range
413 of $26.4\text{-}26.9\ \sigma_t$ in Fig. 2b). It appeared likely that the Oyashio, which carries low salinity, low
414 DOC but high DIC concentrations, and low $\Delta^{14}\text{C-DIC}$ values in the subarctic intermediate water,
415 influenced the upper layers (above 1000 m) at Sta B2. The Oyashio water could further intruded
416 southward to affect the upper 200-1000 m at Sta A4 and mixed with the Kuroshio water to form
417 the KE water mass flowing eastward, which resulted in low DOC, high DIC and low $\Delta^{14}\text{C-DIC}$
418 values. However, it cannot be determined whether this southward intrusion of Oyashio water is
419 seasonal or decadal oscillations (Ding et al., 2018). Previous studies focused on physical

420 oceanography have shown that the unstable mode of the KE could generate active water-mass
421 changes around the region, such as the enhanced meso-scale eddies and ocean recirculation
422 (Qiu and Chen, 2005; Qiu and Chen, 2011; Ma et al., 2016). The fresher Oyashio-origin water
423 could be transported southward through the meso-scale eddies (Qiu and Chen, 2011),
424 influencing the chemical and biological processes in the KE region. Using the significantly low
425 $\Delta^{14}\text{C}$ -DIC values at stations B2 and A4 in the upper 700 m depth in the KE region, we also
426 demonstrated the same strong influence of the southward Oyashio-transported subarctic
427 intermediate water mass via meso-scale eddies (Ding et al., 2018). The ratios of Oyashio water
428 to Kuroshio water mixing for the five stations (B2, B8, A4, A8 and B9) were obtained by mass
429 balance calculations based on the selected two end-member $\Delta^{14}\text{C}$ -DIC values (an average of
430 50‰ for the Kuroshio water and -220 ‰ for the North Pacific Intermediate Water of Oyashio)
431 in the $\Delta^{14}\text{C}$ -DIC Keeling plot analysis (Fig. 10) (Ding et al., 2018). For example, 55-58%
432 Oyashio water could contribute to produce the observed $\Delta^{14}\text{C}$ -DIC values at the depth of 500
433 m in Stas B2 and B8 and 100% Oyashio water at Sta A4 and 96-100% Kuroshio water at Stas
434 A8 and B9, respectively. If we consider that the distribution of DOC is controlled mainly by
435 hydrodynamic mixing in the KE region, the conservative concentrations of DOC could
436 subsequently be calculated using the two water mass mixing model and the corresponding
437 average DOC values for the selected end-member water masses (an average of 57 μM for the
438 Kuroshio water and 40 μM for the NPIW of Oyashio) derived from the $\Delta^{14}\text{C}$ -DIC values within
439 the range of 40-56 μM . The difference between the measured and conservative DOC (DOC^0)
440 concentrations ($\Delta\text{DOC}=\text{DOC}_{\text{measured}} - \text{DOC}^0$) can represent other biological processes that
441 secondarily modulate DOC in the KE region. For example, the positive ΔDOC values ($\sim 6 \mu\text{M}$)
442 that accounted for approximately 11% of the measured DOC at Sta B8 indicated a net DOC
443 increase from biological processes, accompanied by the relatively low DIC concentrations
444 shown in Fig. 9c. The recirculation gyre immediately south of the KE has been found to exhibit

445 high production rates in winter-spring season in the North Pacific due to the entrainment of
446 nutrient-rich water during deep winter mixing (Yasunaka et al., 2013; Yasunaka et al., 2014).
447 However, biological consumptions of DOC could account for 8-20% of the total DOC pool
448 based on the negative Δ DOC values (2-8 μ M) and the measured DOC at Stas B2 and A4.

449 The concentrations of DOC in deep waters in the KE region were low, in the range of 36-44
450 μ M, comparable to the values reported for the deep North Pacific (Druffel et al., 1992; Hansell
451 and Carlson, 1998; Hansell et al., 2009) and the deep South Pacific (34-43 μ M) (Doval and
452 Hansell, 2000; Druffel and Griffin, 2015) but slightly lower than the values in the North Atlantic
453 (40-48 μ M) (Carlson et al., 2010; Druffel et al., 2016). These uniformly low levels of DOC
454 indicate the homogeneous distribution of deep water and the more presumably refractory DOC
455 left behind in deeper waters in the KE and North Pacific (Carlson et al., 2010; Hansell et al.,
456 2012; Follett et al., 2014). Radiocarbon measurements of DOC collected in the KE indicate that
457 the 14 C age of DOC in deep water was \sim 6,200 years (Wang, unpublished data), similar to the
458 DOC ages in the deep North Pacific (Druffel et al., 1992), and support the refractory nature of
459 DOC in the deep KE. The lower deep DOC concentrations in the North Pacific relative to the
460 North Atlantic could be due to the general circulation pattern of the world ocean, as proposed
461 by Hansell and Carlson (1998). DOC has been cycled for longer time scales with older 14 C ages
462 (\sim 6,000 years) in the deep North Pacific (Druffel et al., 1992) than DOC (\sim 4,000 years) in the
463 North Atlantic Ocean (Bauer et al., 1992). However, by comparing with the deep DOC results
464 in the slope region of the ECS, it can be observed that the deep DOC level in the KE was 10-
465 15 μ M lower on average than that in the ECS, implying the possibility of outflow export of
466 DOC from marginal seas to the ocean interior and cycling in the deep ocean for a long duration.

467 **5 Summary**

468 The results of our study indicate that the concentration of DOC ranged from 45 to 88 μ M in
469 the outer shelf and the slope region of ECS and from 35 to 65 μ M in the KE region. The

470 distribution of DOC in the shelf-edge and slope region of the ECS was largely influenced by
471 the physical mixing processes of Kuroshio and ECS shelf waters. The upwelling intrusion of
472 Kuroshio intermediate water could dilute the DOC concentrations at stations around the shelf
473 break region of the ECS.

474 In comparison, the concentrations of DOC in the KE region were significantly lower in the
475 surface layer. The DOC in the deep water of the KE had similar comparable values as those
476 reported for the deep north and south Pacific. The large spatial variations of DOC in the upper
477 700 m among the stations in the KE were influenced primarily by hydrodynamic mixing of two
478 different water masses. The Kuroshio, which carries warm and relatively higher DOC water,
479 and the Oyashio, which carries cold and fresh subarctic intermediate water with lower DOC,
480 mix to form KE. These mixing dynamics could have a major influence on primary production
481 and on biogeochemical processes in the KE region.

482

483

484 *Data availability.* All data used in this study will be freely available, for scientific use only,
485 upon request. Anyone interested in using this data set for scientific research should contact the
486 corresponding author via e-mail.

487

488

489

490 *Author contributions.* Ling Ding is a post-doc working on this project, participated in the cruises,
491 sample analysis and manuscript writing. Tiantian Ge is a laboratory technician participated in
492 all cruises, sampling and sample analysis. Dr. Xuchen Wang is the corresponding author and
493 leading scientist for this study from proposal writing, cruise and sampling planning, and
494 manuscript writing. All authors have read the manuscript and agreed on the authorship.

495

496

497

498 *Competing interests.* The authors declare that they have no conflict of interest.

499

500

501

502 *Acknowledgments.* We thank Drs. Lixin Wu and Jing Zhang for providing the ECS and KE
503 cruise opportunity and Drs. Huiwang Gao and Lei Li for the help during sample collection. We
504 thank Yuejun Xue, Chunle Luo, Caili Xu, Yuanzhi Qi and Sen Shan for help and assistance
505 during sample analysis in laboratory. We give our special thanks to the Captains and crew
506 members of *R/V Dongfanghong-2* and *R/V Shinset Maru* for help during the cruises. We thank
507 the Associate Editor and three reviewers for the valuable and constructive comments that
508 greatly improved the manuscript. Financial support for this work was provided by the National
509 Natural Science Foundation of China (grant numbers: 91858210 and 91428101) and the
510 Fundamental Research Funds for the Central Universities (grant number: 201762009).

511

512

513

514 **References**

515 Azam, F., Fenchel, T., Field, J. G., Gray, J., Meyer-Reil, L. and Thingstad, F.: The ecological role of
516 water-column microbes in the sea, *Mar. Ecol Prog Ser.*, 20, 257-263, 1983.

517 Bauer, J. E. and Bianchi, T. S.: Dissolved organic carbon cycling and transformation, in: *Treatise on*
518 *Estuarine and Coastal Science*, edited by: Wolanski, E. and McLusky, D., 7-67, Academic Press,
519 Waltham, 2011.

520 Bauer, J. E., Cai, W.-J., Raymond, P. A., Bianchi, T. S., Hopkinson, C. S. and Regnier, P. A. G.: The
521 changing carbon cycle of the coastal ocean, *Nature*, 504, 61-70, [http://doi.org/doi:10.1038/nature](http://doi.org/doi:10.1038/nature12857)
522 12857, 2013.

523 Bauer, J. E., Williams, P. M. and Druffel, E. R. M.: ¹⁴C activity of dissolved organic carbon fractions in
524 the north-central Pacific and Sargasso Sea, *Nature*, 357, 667-670, 1992.

525 Bercovici, S. K. and Hansell, D. A.: Dissolved organic carbon in the deep Southern Ocean: Local versus
526 distant controls, *Global Biogeochem. Cycles*, 30, 350-360, <http://doi.org/10.1002/2015GB005252>,
527 2016.

528 Carlson, C. A., Ducklow, H. W., Hansell, D. A. and Smith, W. O.: Organic carbon partitioning during
529 spring phytoplankton blooms in the Ross Sea polynya and the Sargasso Sea, *Limnol. Oceanogr.*, 43,
530 375-386, <http://doi.org/10.4319/lo.1998.43.3.0375>, 1998.

531 Carlson, C. A., Ducklow, H. W. and Michaels, A. F.: Annual flux of dissolved organic carbon from the
532 euphotic zone in the northwestern Sargasso Sea, *Nature*, 371, 405-408, [http://doi.org/10.1038/371405](http://doi.org/10.1038/371405a0)
533 a0, 1994.

534 Carlson, C. A., Hansell, D. A., Nelson, N. B., Siegel, D. A., Smethie, W. M., Khatiwala, S., Meyers, M.
535 M. and Halewood, E.: Dissolved organic carbon export and subsequent remineralization in the

536 mesopelagic and bathypelagic realms of the North Atlantic basin, *Deep-Sea Res. Pt. II*, 57, 1433-
537 1445, <http://doi.org/10.1016/j.dsr2.2010.02.013>, 2010.

538 Catal á T. S., Reche, I., Álvarez, M., Khatiwala, S., Guallart, E. F., Ben fez-Barrios, V. M., Fuentes-
539 Lema, A., Romera-Castillo, C., Nieto-Cid, M., Pelejero, C., Fraile-Nuez, E., Ortega-Retuerta, E.,
540 Marras é C. and Álvarez-Salgado, X. A.: Water mass age and aging driving chromophoric dissolved
541 organic matter in the dark global ocean, *Global Biogeochem. Cycles*, 29, 917-934,
542 <http://doi.org/10.1002/2014GB005048>, 2015a.

543 Catal á T. S., Reche, I., Fuentes-Lema, A., Romera-Castillo, C., Nieto-Cid, M., Ortega-Retuerta, E.,
544 Calvo, E., Álvarez, M., Marras é C., Stedmon, C. A. and Álvarez-Salgado, X. A.: Turnover time of
545 fluorescent dissolved organic matter in the dark global ocean, *Nat. Commun.*, 6, 5986,
546 <http://doi.org/10.1038/ncomms6986>, 2015b.

547 Chen, C.-T. A. and Wang, S.-L.: Carbon, alkalinity and nutrient budgets on the East China Sea
548 continental shelf, *J. Geophys. Res.: Oceans*, 104, 20675-20686, <http://doi.org/10.1029/1999jc900055>,
549 1999.

550 Dai, M., Meng, F., Tang, T., Kao, S.-J., Lin, J., Chen, J., Huang, J.-C., Tian, J., Gan, J. and Yang, S.:
551 Excess total organic carbon in the intermediate water of the South China Sea and its export to the
552 North Pacific, *Geochem. Geophys. Geosyst.*, 10, Q12002, <http://doi.org/10.1029/2009GC002752>,
553 2009.

554 Ding, L., Ge, T., Gao, H., Luo, C., Xue, Y., Druffel, E. R. M. and Wang, X.: Large variability of dissolved
555 inorganic radiocarbon in the Kuroshio Extension of the northwest North Pacific, *Radiocarbon*, 60,
556 691-704, <http://doi.org/10.1017/RDC.2017.143>, 2018.

557 Doval, M. D. and Hansell, D. A.: Organic carbon and apparent oxygen utilization in the western South
558 Pacific and the central Indian Oceans, *Mar. Chem.*, 68, 249-264, [http://doi.org/10.1016/S0304-4203\(99\)00081-X](http://doi.org/10.1016/S0304-4203(99)00081-X), 2000.

560 Druffel, E. R. M. and Griffin, S.: Radiocarbon in dissolved organic carbon of the South Pacific Ocean,
561 *Geophys. Res. Lett.*, 42, 4096-4101, <http://doi.org/10.1002/2015GL063764>, 2015.

562 Druffel, E. R. M., Griffin, S., Coppola, A. I. and Walker, B. D.: Radiocarbon in dissolved organic carbon
563 of the Atlantic Ocean, *Geophys. Res. Lett.*, 43, 5279-5286, <http://doi.org/10.1002/2016GL068746>,
564 2016.

565 Druffel, E. R. M., Griffin, S., Wang, N., Garcia, N. G., McNichol, A. P., Key, R. M. and Walker, B. D.:
566 Dissolved organic radiocarbon in the Central Pacific Ocean, *Geophys. Res. Lett.*, 46, 5396-5403,
567 <http://doi.org/10.1029/2019GL083149>, 2019.

568 Druffel, E. R., Williams, P. M., Bauer, J. E. and Ertel, J. R.: Cycling of dissolved and particulate organic
569 matter in the open ocean, *J. Geophys. Res.*, 97, 15639-15659, 1992.

570 Fassbender, A. J., Sabine, C. L., Cronin, M. F. and Sutton, A. J.: Mixed-layer carbon cycling at the
571 Kuroshio Extension Observatory, *Global Biogeochem. Cycles*, 31, 272-288, <http://doi.org/10.1002/2016GB005547>, 2017.

573 Fenchel, T.: The microbial loop-25 years later, *J. Exp. Mar. Bio. Ecol.*, 366, 99-103, <http://doi.org/10.1016/j.jembe.2008.07.013>, 2008.

575 Follett, C. L., Repeta, D. J., Rothman, D. H., Xu, L. and Santinelli, C.: Hidden cycle of dissolved organic
576 carbon in the deep ocean, *Proc. Natl. Acad. Sci. USA.*, 111, 16706-16711, <http://doi.org/10.1073/pnas.1407445111>, 2014.

578 Gan, S., Wu, Y. and Zhang, J.: Bioavailability of dissolved organic carbon linked with the regional
579 carbon cycle in the East China Sea, *Deep-Sea Res. Pt. II*, 124, 19-28, <http://doi.org/10.1016/j.dsr2.2015.06.024>, 2016.

580 Ge, T., Wang, X., Zhang, J., Luo, C. and Xue, Y.: Dissolved inorganic radiocarbon in the Northwest
581

582 Pacific continental margin, *Radiocarbon*, 58, 517-529, <http://doi.org/10.1017/RDC.2016.23>, 2016.

583 Gong, G.-C., Wen, Y.-H., Wang, B.-W. and Liu, G.-J.: Seasonal variation of chlorophyll a concentration,
584 primary production and environmental conditions in the subtropical East China Sea, *Deep-Sea Res.*
585 *Pt. II*, 50, 1219-1236, [http://doi.org/10.1016/S0967-0645\(03\)00019-5](http://doi.org/10.1016/S0967-0645(03)00019-5), 2003.

586 Guo, L., Santschi, P. H. and Warnken, K. W.: Dynamics of dissolved organic carbon (DOC) in oceanic
587 environments, *Limnol. Oceanogr.*, 40, 1392-1403, <http://doi.org/doi:10.4319/lo.1995.40.8.1392>,
588 1995.

589 Guo, X., Miyazawa, Y. and Yamagata, T.: The Kuroshio onshore intrusion along the shelf break of the
590 East China Sea: The origin of the Tsushima Warm Current, *J. Phys. Oceanogr.*, 36, 2205-2231,
591 <http://doi.org/10.1175/JPO2976.1>, 2006.

592 Hansell, D. A. and Carlson, C. A.: Deep-ocean gradients in the concentration of dissolved organic carbon,
593 *Nature*, 395, 263-266, <http://doi.org/10.1038/26200>, 1998.

594 Hansell, D. A. and Carlson, C. A.: Marine dissolved organic matter and the carbon cycle, *Oceanography*,
595 14, 41-49, 2001.

596 Hansell, D. A., Carlson, C. A., Repeta, D. J. and Schlitzer, R.: Dissolved organic matter in the ocean: A
597 controversy stimulates new insights, *Oceanography*, 22, 202-211, <http://doi.org/10.5670/oceanog.2009.109>, 2009.

598
599 Hansell, D. A., Carlson, C. A. and Schlitzer, R.: Net removal of major marine dissolved organic carbon
600 fractions in the subsurface ocean, *Global Biogeochem. Cycles*, 26, GB1016, <http://doi.org/10.1029/2011gb004069>, 2012.

601
602 Hansell, D. A., Carlson, C. A. and Suzuki, Y.: Dissolved organic carbon export with North Pacific
603 Intermediate Water formation, *Global Biogeochem. Cycles*, 16, 1007, <http://doi.org/10.1029/2000GB001361>, 2002.

604
605 Hansell, D. A. and Peltzer, E. T.: Spatial and temporal variations of total organic carbon in the Arabian
606 Sea, *Deep-Sea Res. Pt. II*, 45, 2171-2193, [http://doi.org/doi:10.1016/S0967-0645\(98\)00067-8](http://doi.org/doi:10.1016/S0967-0645(98)00067-8), 1998.

607 Hansell, D. A. and Waterhouse, T. Y.: Controls on the distributions of organic carbon and nitrogen in the
608 eastern Pacific Ocean, *Deep-Sea Res. Pt. I*, 44, 843-857, [http://doi.org/10.1016/S0967-0637\(96\)](http://doi.org/10.1016/S0967-0637(96)00128-8)
609 00128-8, 1997.

610 Hsueh, Y.: The Kuroshio in the East China Sea, *J. Mar. Syst.*, 24, 131-139, [http://doi.org/10.1016/S0924-](http://doi.org/10.1016/S0924-7963(99)00083-4)
611 7963(99)00083-4, 2000.

612 Hu, D., Wu, L., Cai, W., Gupta, A. S., Ganachaud, A., Qiu, B., Gordon, A. L., Lin, X., Chen, Z., Hu, S.,
613 Wang, G., Wang, Q., Sprintall, J., Qu, T., Kashino, Y., Wang, F. and Kessler, W. S.: Pacific western
614 boundary currents and their roles in climate, *Nature*, 522, 299-308, [http://doi.org/10.1038/nature](http://doi.org/10.1038/nature14504)
615 14504, 2015.

616 Hung, J. J., Chen, C. H., Gong, G. C., Sheu, D. D. and Shiah, F. K.: Distributions, stoichiometric patterns
617 and cross-shelf exports of dissolved organic matter in the East China Sea, *Deep-Sea Res. Pt. II*, 50,
618 1127-1145, [http://doi.org/10.1016/S0967-0645\(03\)00014-6](http://doi.org/10.1016/S0967-0645(03)00014-6), 2003.

619 Hung, J. J., Wang, S. M. and Chen, Y. L.: Biogeochemical controls on distributions and fluxes of
620 dissolved and particulate organic carbon in the Northern South China Sea, *Deep-Sea Res. Pt. II*, 54,
621 1486-1503, <http://doi.org/10.1016/j.dsr2.2007.05.006>, 2007.

622 Ma, X., Zhao, J., Chang, P., Liu, X., Montuoro, R., Small, R. J., Bryan, F. O., Greatbatch, R. J., Brandt,
623 P., Wu, D., Lin, X. and Wu, L.: Western boundary currents regulated by interaction between ocean
624 eddies and the atmosphere, *Nature*, 535, 533-537, <http://doi.org/10.1038/nature18640>, 2016.

625 McNichol, A. P., Jones, G. A., Hutton, D. L., Gagnon, A. R. and Key, R. M.: The rapid preparation of
626 seawater ΣCO_2 for radiocarbon analysis at the National Ocean Sciences AMS Facility, *Radiocarbon*,
627 36, 237-246, 1994.

628 Nelson, C. E. and Carlson, C. A.: Tracking differential incorporation of dissolved organic carbon types
629 among diverse lineages of Sargasso Sea bacterioplankton, *Environ Microbiol.*, 14, 1500-1516,
630 <http://doi.org/10.1111/j.1462-2920.2012.02738.x>, 2012.

631 Nishibe, Y., Takahashi, K., Sato, M., Kodama, T., Kakehi, S., Saito, H. and Furuya, K.: Phytoplankton
632 community structure, as derived from pigment signatures, in the Kuroshio Extension and adjacent
633 regions in winter and spring, *J Oceanogr.*, 73, 463-478, <http://doi.org/10.1007/s10872-017-0415-3>,
634 2017.

635 Nishibe, Y., Takahashi, K., Shiozaki, T., Kakehi, S., Saito, H. and Furuya, K.: Size-fractionated primary
636 production in the Kuroshio Extension and adjacent regions in spring, *J Oceanogr.*, 71, 27-40, <http://doi.org/10.1007/s10872-014-0258-0>, 2015.

637
638 Nishikawa, H., Yasuda, I. and Itoh, S.: Impact of winter-to-spring environmental variability along the
639 Kuroshio jet on the recruitment of Japanese sardine (*Sardinops melanostictus*), *Fish. Oceanogr.*, 20,
640 570-582, <http://doi.org/10.1111/j.1365-2419.2011.00603.x>, 2011.

641 Ogawa, H., Fukuda, R. and Koike, I.: Vertical distributions of dissolved organic carbon and nitrogen in
642 the Southern Ocean, *Deep-Sea Res. Pt. I*, 46, 1809-1826, [http://doi.org/10.1016/S0967-0637\(99\)](http://doi.org/10.1016/S0967-0637(99)00027-8)
643 00027-8, 1999.

644 Ogawa, H. and Tanoue, E.: Dissolved Organic Matter in oceanic waters, *J Oceanogr.*, 59, 129-147,
645 <http://doi.org/10.1023/a:1025528919771>, 2003.

646 Ogawa, H., Usui, T. and Koike, I.: Distribution of dissolved organic carbon in the East China Sea, *Deep-*
647 *Sea Res. Pt. II*, 50, 353-366, [http://doi.org/10.1016/S0967-0645\(02\)00459-9](http://doi.org/10.1016/S0967-0645(02)00459-9), 2003.

648 Qiu, B.: Kuroshio and Oyashio currents, in: *Encyclopedia of Ocean Science*, edited by: Steele, J. H.,
649 Turekian, K. K. and Thorpe, S. A., 1413-1425, Academic Press, San Diego, 2001.

650 Qiu, B. and Chen, S.: Variability of the Kuroshio Extension Jet, recirculation gyre, and mesoscale eddies
651 on decadal time scales, *J. Phys. Oceanogr.*, 35, 2090-2103, <http://doi.org/10.1175/jpo2807.1>, 2005.

652 Qiu, B. and Chen, S.: Effect of decadal Kuroshio Extension Jet and eddy variability on the modification
653 of North Pacific Intermediate Water, *J. Phys. Oceanogr.*, 41, 503-515, [http://doi.org/10.1175/](http://doi.org/10.1175/2010JPO4575.1)
654 2010JPO4575.1, 2011.

655 Riedel, T. and Dittmar, T.: A method detection limit for the analysis of natural organic matter via Fourier
656 Transform Ion Cyclotron Resonance Mass Spectrometry, *Anal Chem.*, 86, 8376-8382, [http://doi.org](http://doi.org/10.1021/ac501946m)
657 /10.1021/ac501946m, 2014.

658 Sharp, J. H., Benner, R., Bennett, L., Carlson, C. A., Fitzwater, S. E., Peltzer, E. T. and Tupas, L. M.:
659 Analyses of dissolved organic carbon in seawater: the JGOFS EqPac methods comparison, *Mar.*
660 *Chem.*, 48, 91-108, [http://doi.org/10.1016/0304-4203\(94\)00040-K](http://doi.org/10.1016/0304-4203(94)00040-K), 1995.

661 Sharp, J. H., Carlson, C. A., Peltzer, E. T., Castle-Ward, D. M., Savidge, K. B. and Rinker, K. R.: Final
662 dissolved organic carbon broad community intercalibration and preliminary use of DOC reference
663 materials, *Mar. Chem.*, 77, 239-253, [http://doi.org/10.1016/S0304-4203\(02\)00002-6](http://doi.org/10.1016/S0304-4203(02)00002-6), 2002.

664 Stuiver, M. and Polach, H. A.: Discussion reporting of ¹⁴C data, *Radiocarbon*, 19, 355-363, [http://doi.](http://doi.org/10.1017/S0033822200003672)
665 [org/10.1017/S0033822200003672](http://doi.org/10.1017/S0033822200003672), 1977.

666 Talley, L. D.: North Pacific Intermediate Water transports in the mixed water region, *J. Phys. Oceanogr.*,
667 27, 1795-1803, [http://doi.org/10.1175/1520-0485\(1997\)027<1795:npiwti>2.0.co;2](http://doi.org/10.1175/1520-0485(1997)027<1795:npiwti>2.0.co;2), 1997.

668 Tsunogai, S., Ono, T. and Watanabe, S.: Increase in total carbonate in the western North Pacific water
669 and a hypothesis on the missing sink of anthropogenic carbon, *J Oceanogr.*, 49, 305-315, <http://doi.org/10.1007/bf02269568>, 1993.

670
671 Wang, X., Ma, H., Li, R., Song, Z. and Wu, J.: Seasonal fluxes and source variation of organic carbon
672 transported by two major Chinese Rivers: The Yellow River and Changjiang (Yangtze) River, *Global*
673 *Biogeochem. Cycles*, 26, GB2025, <http://doi.org/10.1029/2011GB004130>, 2012.

674 Ward, N. D., Bianchi, T. S., Medeiros, P. M., Seidel, M., Richey, J. E., Keil, R. G. and Sawakuchi, H.
675 O.: Where carbon goes when water flows: Carbon cycling across the aquatic continuum, *Front. Mar.*
676 *Sci.*, 4, <http://doi.org/doi:10.3389/fmars.2017.00007>, 2017.

677 Wong, G. T. F., Tseng, C.-M., Wen, L.-S. and Chung, S.-W.: Nutrient dynamics and N-anomaly at the
678 SEATS station, *Deep-Sea Res. Part II*, 54, 1528-1545, <http://doi.org/doi:10.1016/j.dsr2.2007.05.011>,
679 2007.

680 Wu, L., Cai, W., Zhang, L., Nakamura, H., Timmermann, A., Joyce, T., McPhaden, M. J., Alexander,
681 M., Qiu, B., Visbeck, M., Chang, P. and Giese, B.: Enhanced warming over the global subtropical
682 western boundary currents, *Nature Clim. Change*, 2, 161-166, <http://doi.org/10.1038/nclimate1353>,
683 2012.

684 Wu, K., Dai, M., Li, X., Meng, F., Chen, J. and Lin, J.: Dynamics and production of dissolved organic
685 carbon in a large continental shelf system under the influence of both river plume and coastal
686 upwelling, *Limnol. Oceanogr.*, 62, 973-988, <http://doi.org/doi:10.1002/lno.10479>, 2017.

687 Xu, C., Xue, Y., Qi, Y. and Wang, X.: Quantities and fluxes of dissolved and particulate black carbon in
688 the Changjiang and Huanghe Rivers, China, *Estuar Coast.*, 39, 1617-1625, <http://doi.org/10.1007/s12237-016-0122-0>, 2016.

690 Xue, Y., Zou, L., Ge, T. and Wang, X.: Mobilization and export of millennial-aged organic carbon by
691 the Yellow River, *Limnol. Oceanogr.*, 62, S95-S111, <http://doi.org/10.1002/lno.10579>, 2017.

692 Yang, D., Yin, B., Liu, Z., Bai, T., Qi, J. and Chen, H.: Numerical study on the pattern and origins of
693 Kuroshio branches in the bottom water of southern East China Sea in summer, *J. Geophys. Res.: Oceans*,
694 117, C02014, <http://doi.org/10.1029/2011JC007528>, 2012.

695 Yang, D., Yin, B., Liu, Z. and Feng, X.: Numerical study of the ocean circulation on the East China Sea
696 shelf and a Kuroshio bottom branch northeast of Taiwan in summer, *J. Geophys. Res.: Oceans*, 116,
697 C05015, <http://doi.org/10.1029/2010JC006777>, 2011.

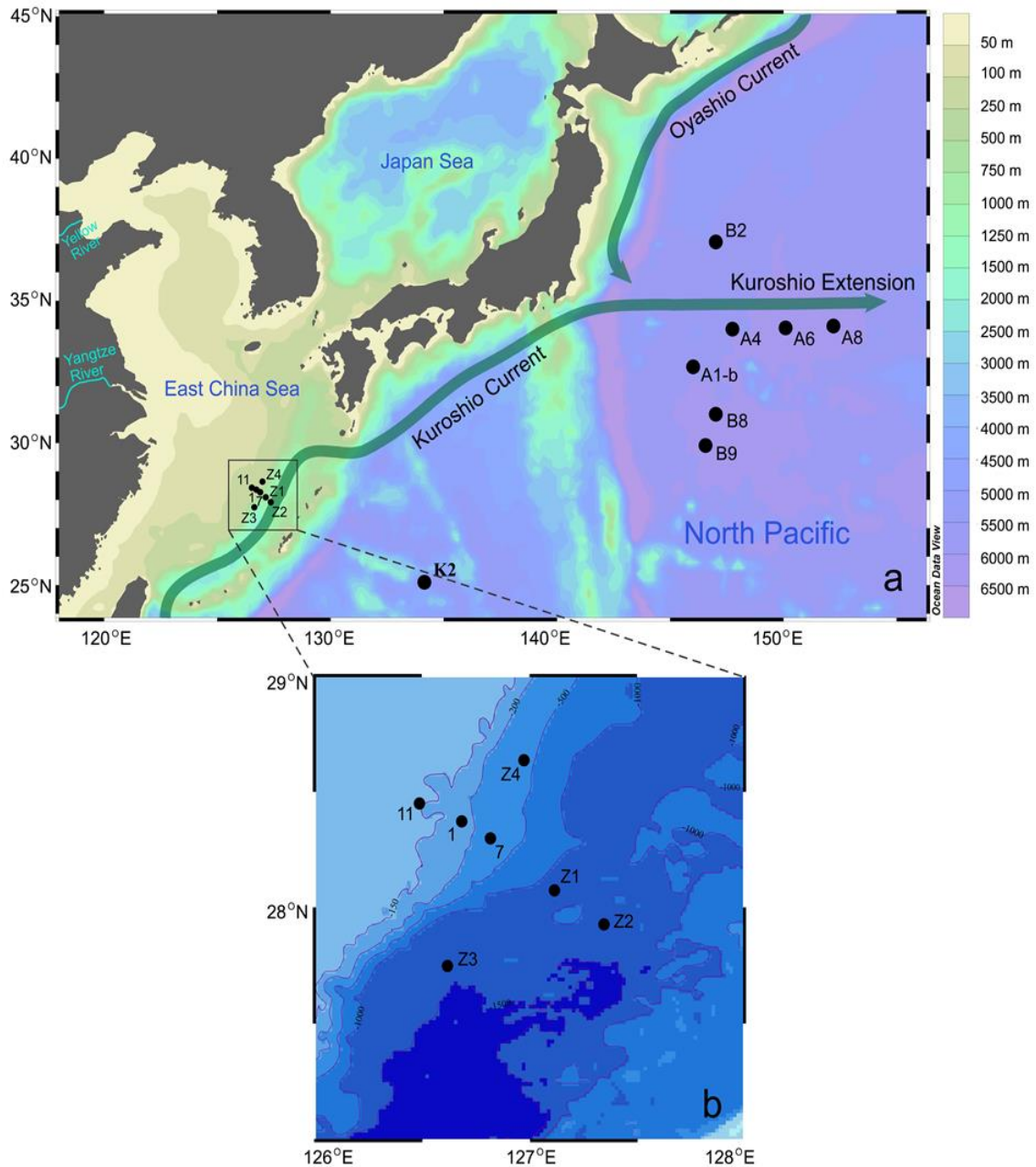
698 Yasuda, I.: Hydrographic structure and variability in the Kuroshio-Oyashio transition area, *J Oceanogr.*,
699 59, 389-402, <http://doi.org/10.1023/a:1025580313836>, 2003.

700 Yasuda, I., Okuda, K. and Shimizu, Y.: Distribution and modification of North Pacific Intermediate
701 Water in the Kuroshio-Oyashio interfrontal zone, *J. Phys. Oceanogr.*, 26, 448-465, [http://doi.org/10.1175/1520-0485\(1996\)026<0448:damonp>2.0.co;2](http://doi.org/10.1175/1520-0485(1996)026<0448:damonp>2.0.co;2), 1996.

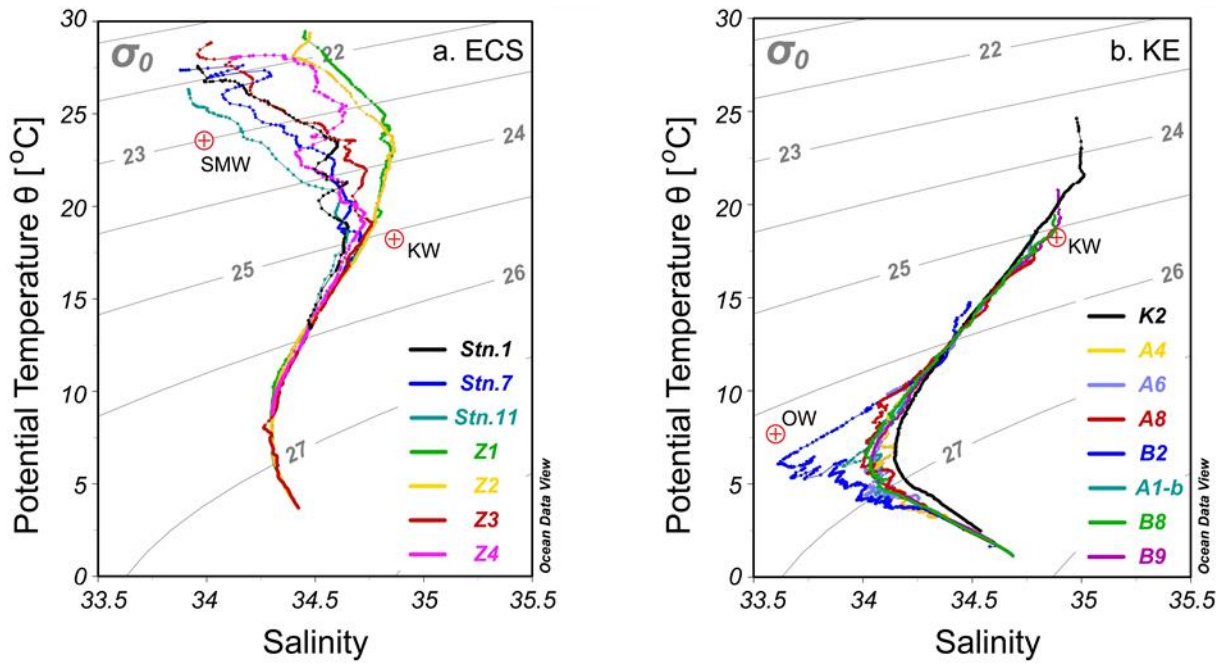
703 Yasunaka, S., Nojiri, Y., Nakaoka, S.-i., Ono, T., Mukai, H. and Usui, N.: Monthly maps of sea surface
704 dissolved inorganic carbon in the North Pacific: Basin-wide distribution and seasonal variation, *J.*
705 *Geophys. Res.: Oceans*, 118, 3843-3850, <http://doi.org/10.1002/jgrc.20279>, 2013.

706 Yasunaka, S., Nojiri, Y., Nakaoka, S.-i., Ono, T., Whitney, F. A. and Telszewski, M.: Mapping of sea
707 surface nutrients in the North Pacific: Basin-wide distribution and seasonal to interannual variability,
708 *J. Geophys. Res.: Oceans*, 119, 7756-7771, <http://doi.org/10.1002/2014JC010318>, 2014.

709



710
 711 **Figure 1.** Map showing the study region and the sampling stations in the ECS and the
 712 northwestern North Pacific during two cruises in 2014-2015 described in the text. Two major
 713 western boundary currents, the northeastward-flowing Kuroshio and southward-flowing
 714 Oyashio, meet and form the Kuroshio Extension flowing eastward to the North Central Pacific.
 715

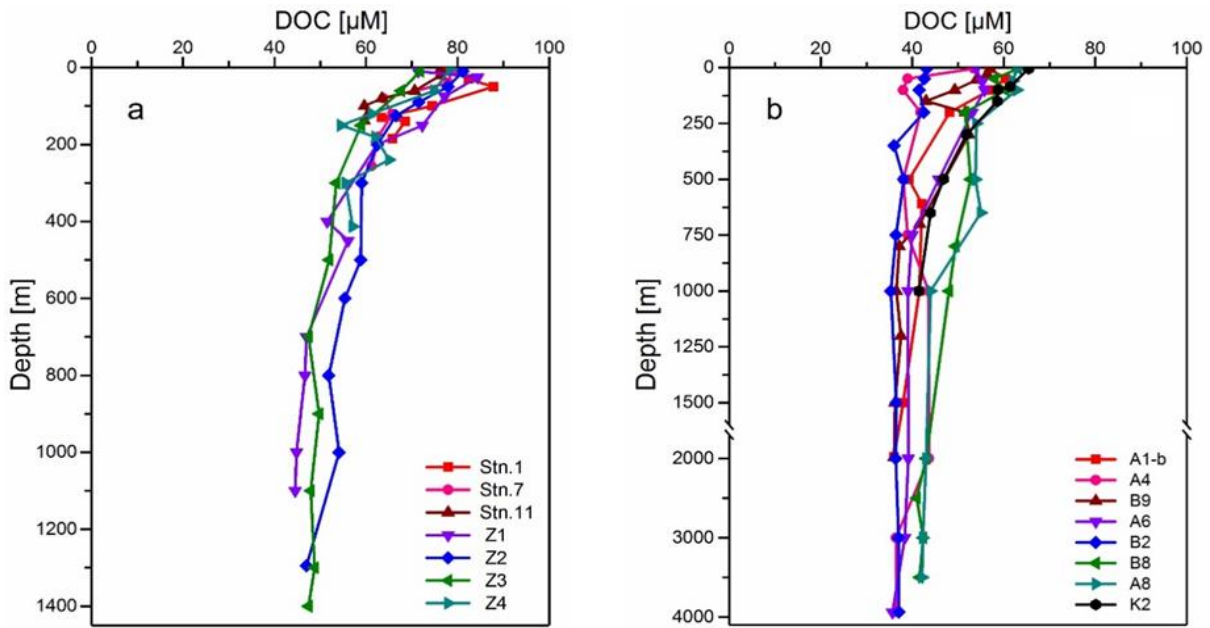


716

717 **Figure 2.** Potential temperature versus salinity (T-S) diagrams for the sampling stations. (a)
 718 Seven shelf-edge to slope stations in the ECS and (b) eight deep stations in the KE region in
 719 the northwestern North Pacific. σ_0 isolines are included in the figures. The coloured lines
 720 correspond to CTD data, and red dots indicate the potential temperature (θ) and salinity (S) of
 721 different water masses. The representative θ and S of these water types referred to previous
 722 studies (Yasuda et al., 1996; Chen and Wang, 1999; Hung et al., 2003; Wong et al., 2007)
 723 Acronyms used in this figure: SMW-Shelf Mixed Water, KW-Kuroshio Water and OW-Oyashio
 724 Water.

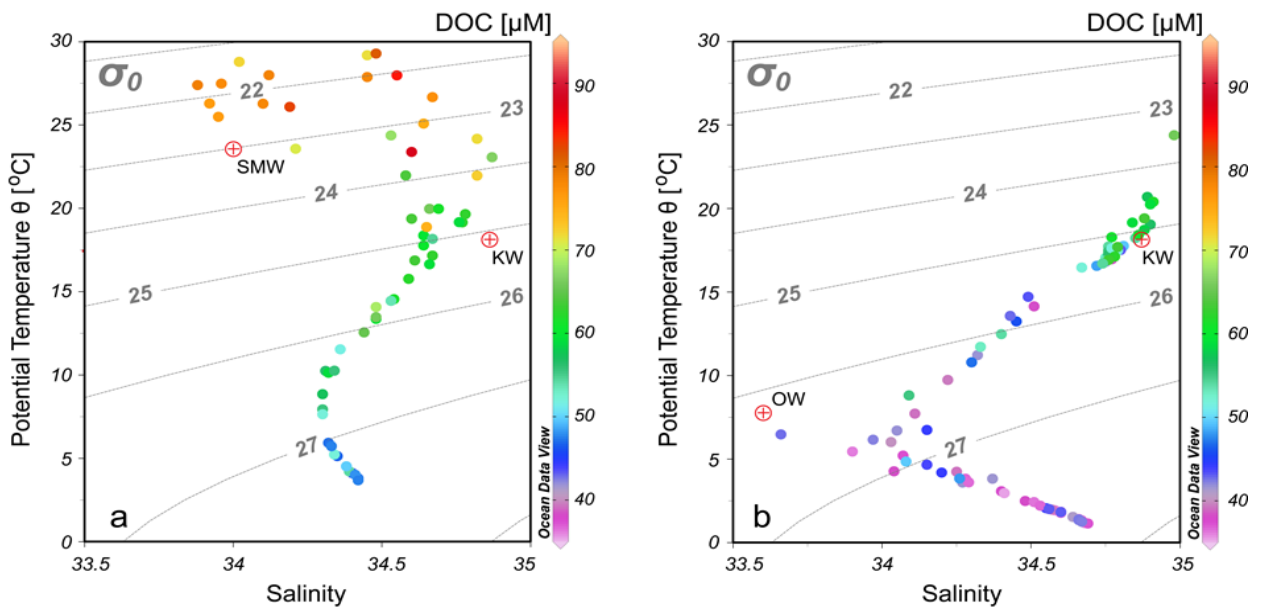
725

726



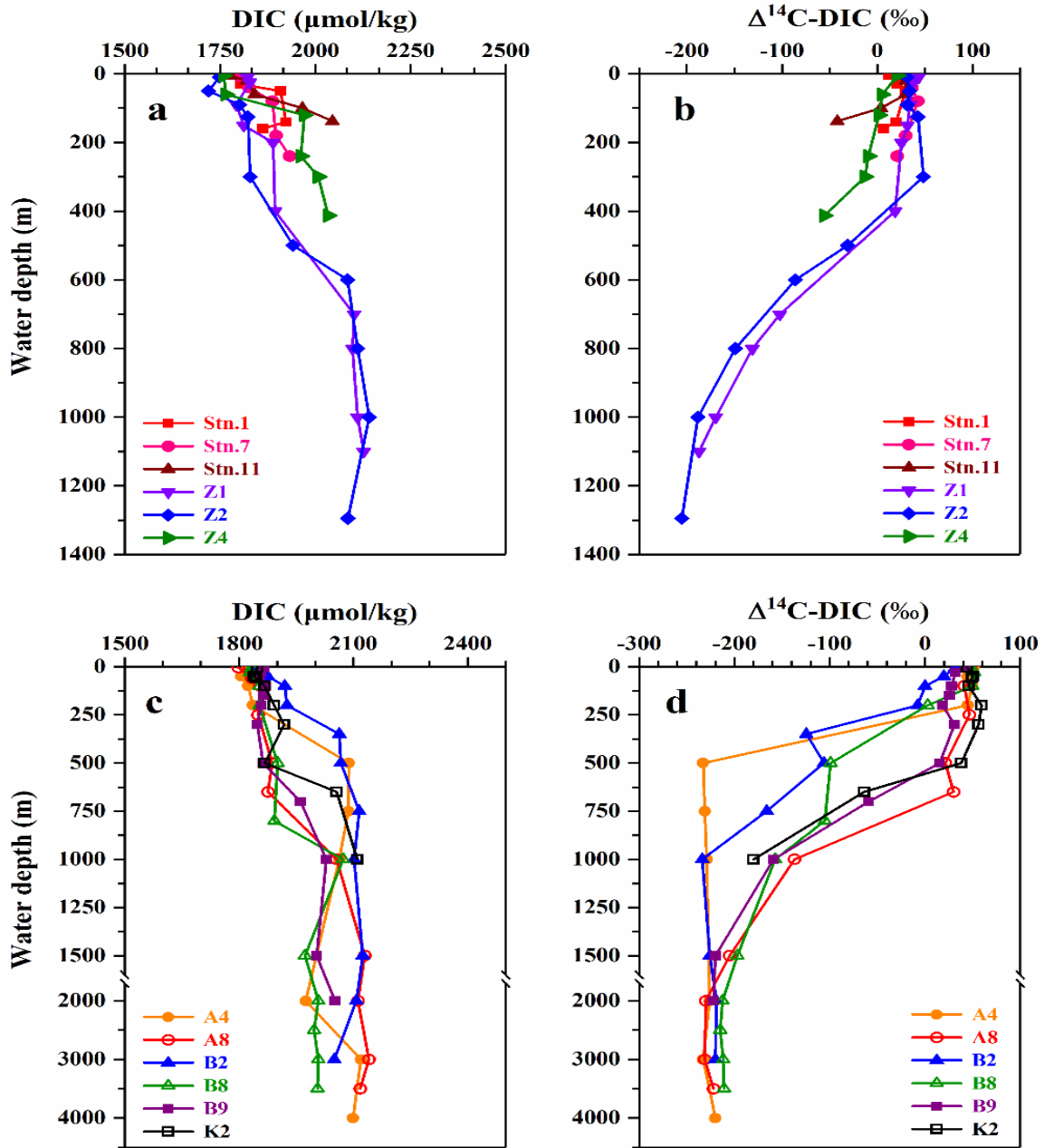
727
 728 **Figure 3.** Depth profiles of DOC concentrations measured for the stations in the (a) ECS and
 729 (b) northwestern North Pacific during the two cruises in 2014-2015. Note in panel b that the
 730 depth below 1500 m is on a different scale.

731
 732



733
 734 **Figure 4.** DOC concentrations superimposed on plots of potential temperature versus salinity
 735 for the sampling stations in the (a) ECS and (b) Kuroshio Extension in the northwestern North
 736 Pacific. σ_0 isolines are included in the figures. Red dots indicate the potential temperature and
 737 salinity of the water types, and acronyms of water types as SMW-Shelf Mixed Water, KW-
 738 Kuroshio Water and OW-Oyashio Water.

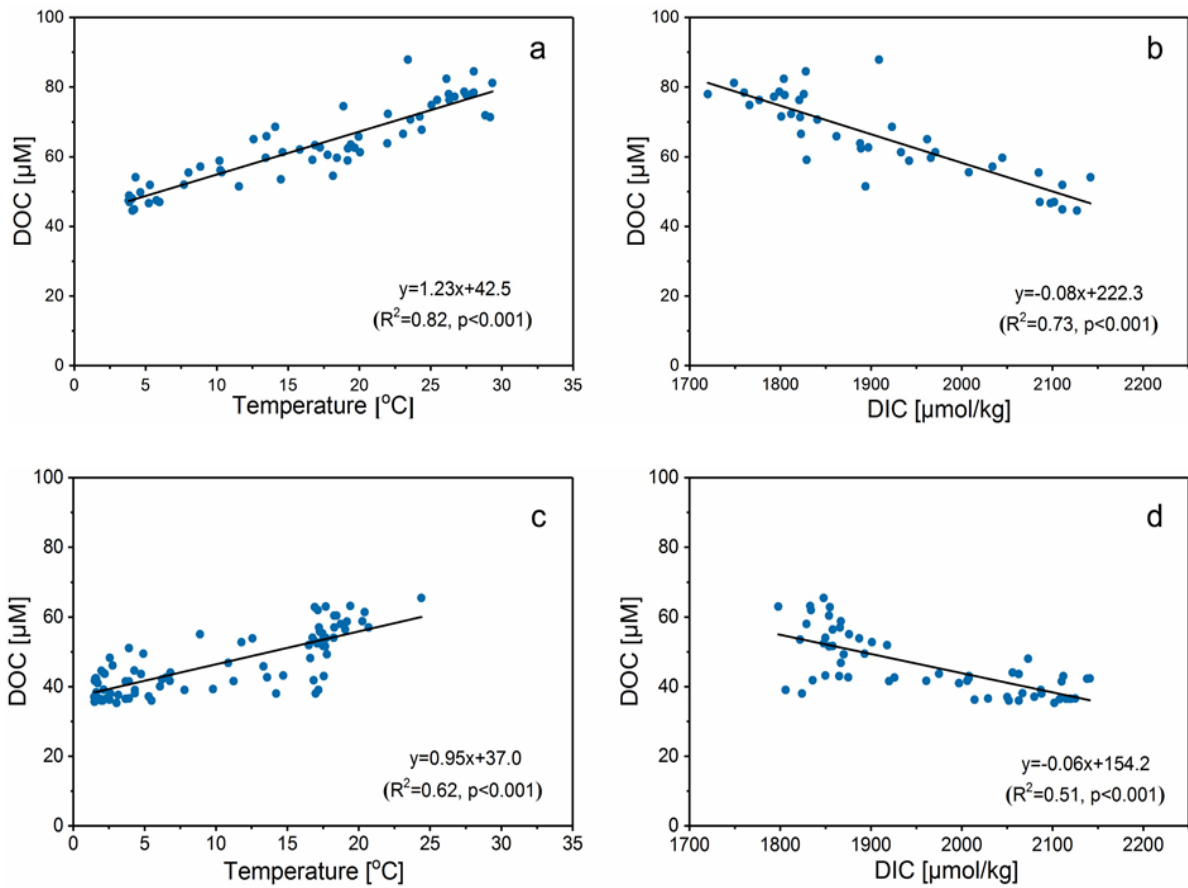
739



740

741 **Figure 5.** Depth profiles of DIC concentrations and $\Delta^{14}\text{C-DIC}$ measured for the stations in the
 742 (a, b) ECS and (c, d) northwestern North Pacific during the two cruises in 2014-2015. Note in
 743 panel c and d that the depth below 1500 m is on a different scale. The plots were adapted from
 744 data previously reported in Ge et al. (2016) and Ding et al. (2018).

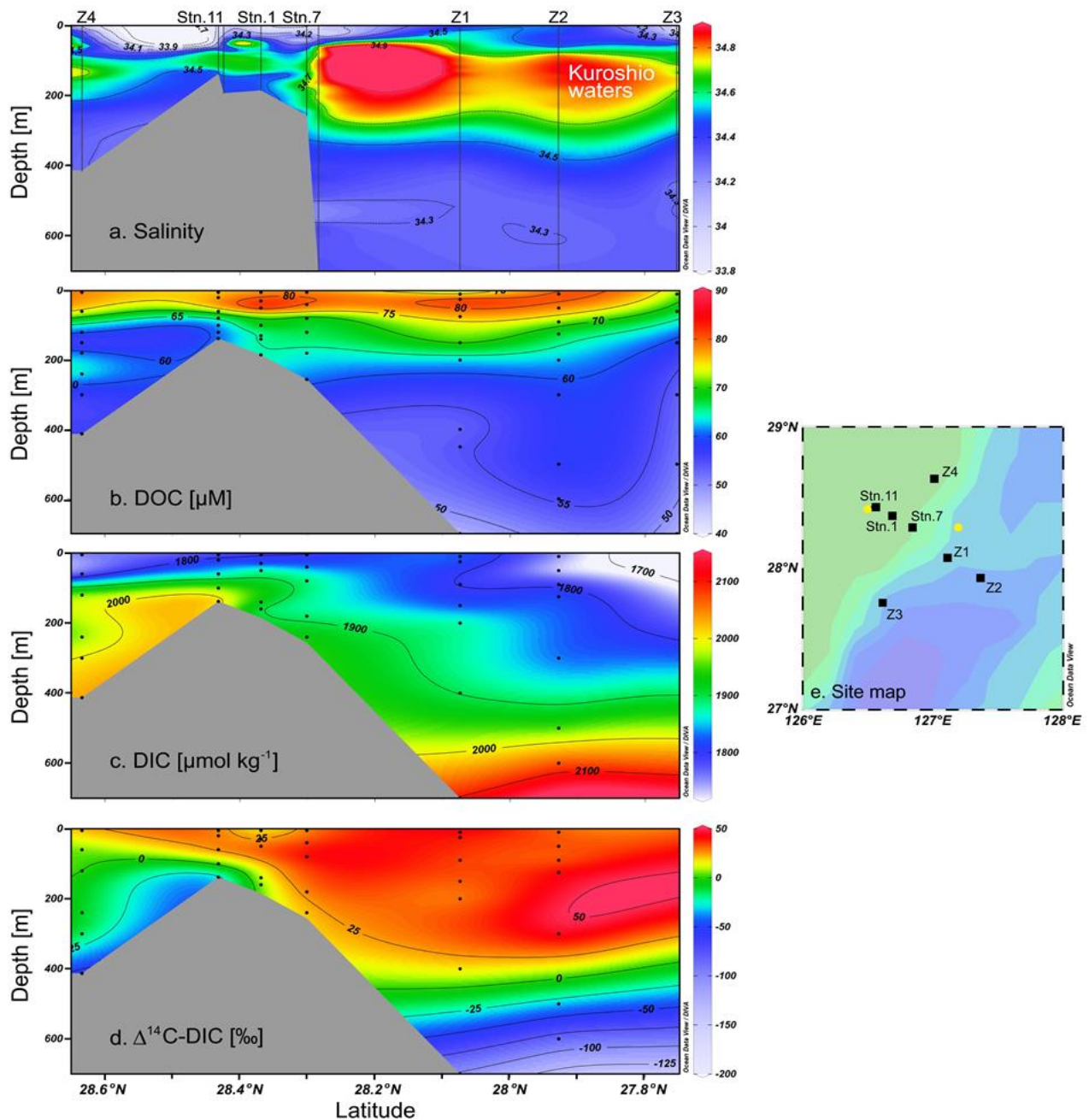
745



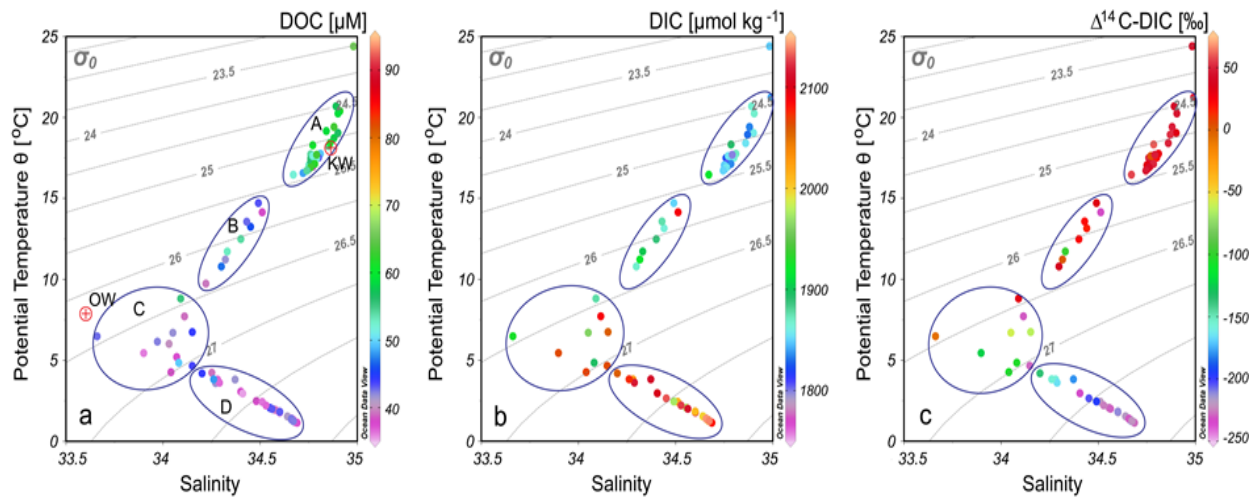
746

747 **Figure 6.** Correlation of DOC concentrations with water temperature and DIC concentrations
 748 for stations sampled in the (a, b) ECS and (c, d) KE. The solid lines denote linear regressions
 749 fit to the data.

750

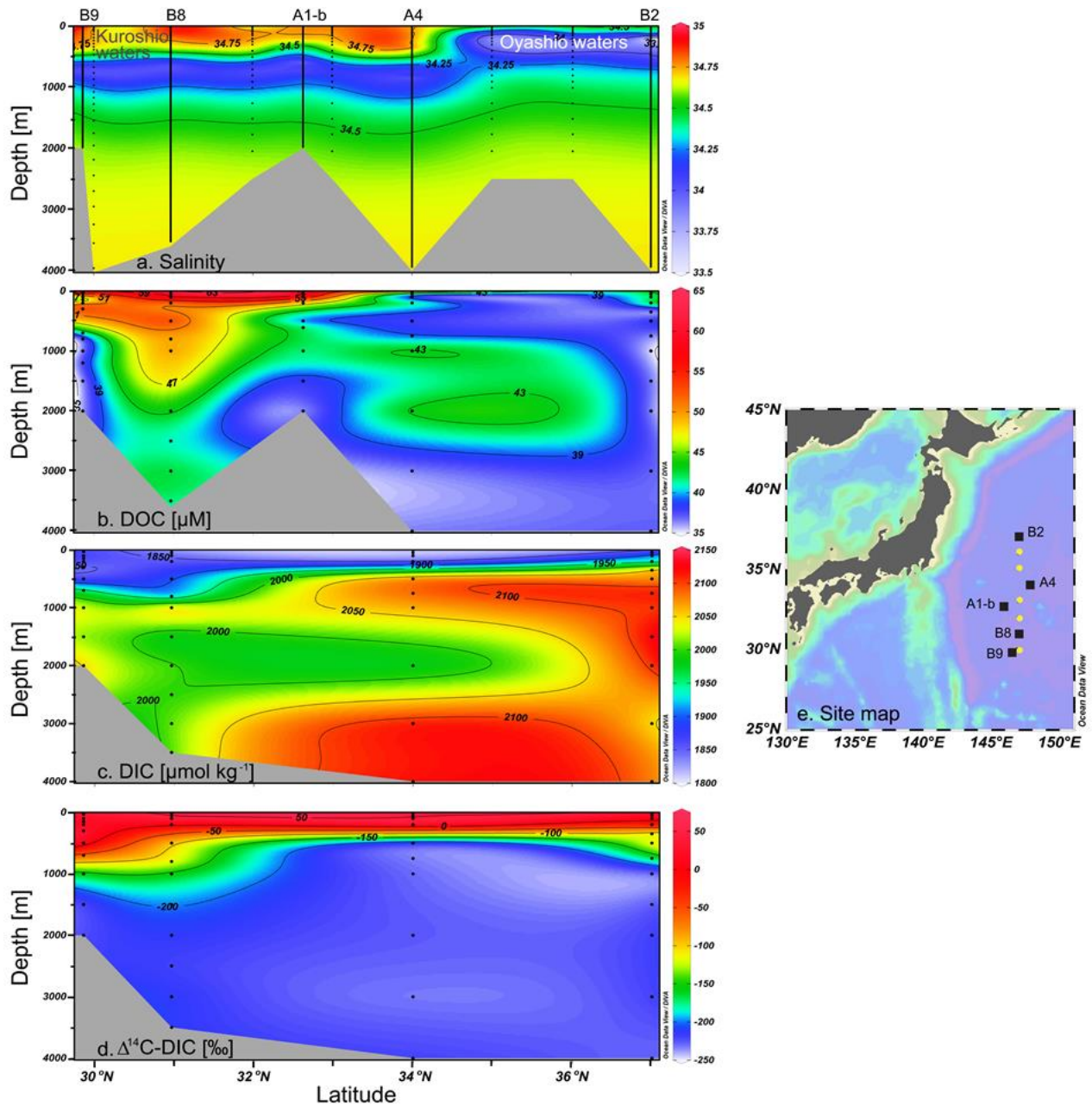


751
 752 **Figure 7.** Transectional distributions of (a) salinity, (b) DOC concentrations, (c) DIC
 753 concentrations and (d) $\Delta^{14}\text{C-DIC}$ values for the (e) sampling stations (black squares) covering
 754 the shelf-edge and slope region of ECS during the cruise in July 2014. Black dots indicate the
 755 depths where samples were collected. Note: (a) The salinity of the other two stations (yellow
 756 circles) from the cruise in July 2011 are included to support the spreading of the data. (b-d) The
 757 distributions of DOC concentrations include seven stations, whereas DIC concentrations and
 758 $\Delta^{14}\text{C-DIC}$ values are given only for six stations due to the lack of data at Sta. Z3 (Ge et al.,
 759 2016).
 760



761
 762 **Figure 8.** Plot of potential temperature (θ) vs. salinity with (a) DOC concentrations, (b) DIC
 763 concentrations and (c) $\Delta^{14}\text{C-DIC}$ values (indicated as the colours of points) associated with the
 764 potential water density (σ_t) for eight stations in the northwestern North Pacific. The circular
 765 areas represent different water masses in terms of (A) lower density water in the upper 300 m
 766 depth with higher DOC concentration, lower DIC concentration and enriched $\Delta^{14}\text{C-DIC}$; (B)
 767 mixed upper water in the 300-500 m depth; (C) mixed intermediated water in 500-800 m water
 768 depth; and (D) denser North Pacific deep water below 1000 m depth. Higher levels of DOC
 769 were associated with lower DIC concentrations, and high $\Delta^{14}\text{C-DIC}$ values were found in lower
 770 density waters ($\sigma_0 < 25.5$, water mass A), while lower levels of DOC were associated with
 771 higher DIC concentrations, and low $\Delta^{14}\text{C-DIC}$ values occurred in denser waters (water mass C
 772 and water mass D at $\sigma_0 > 27.1$). Note: DOC concentrations were measured for all stations,
 773 whereas DIC results from Ding et al. (2018) were only measured for six stations except Stas.
 774 A1-b and A6. Red dots indicate the potential temperature and salinity of the water types, and
 775 acronyms of water types as in Fig. 4 are shown.

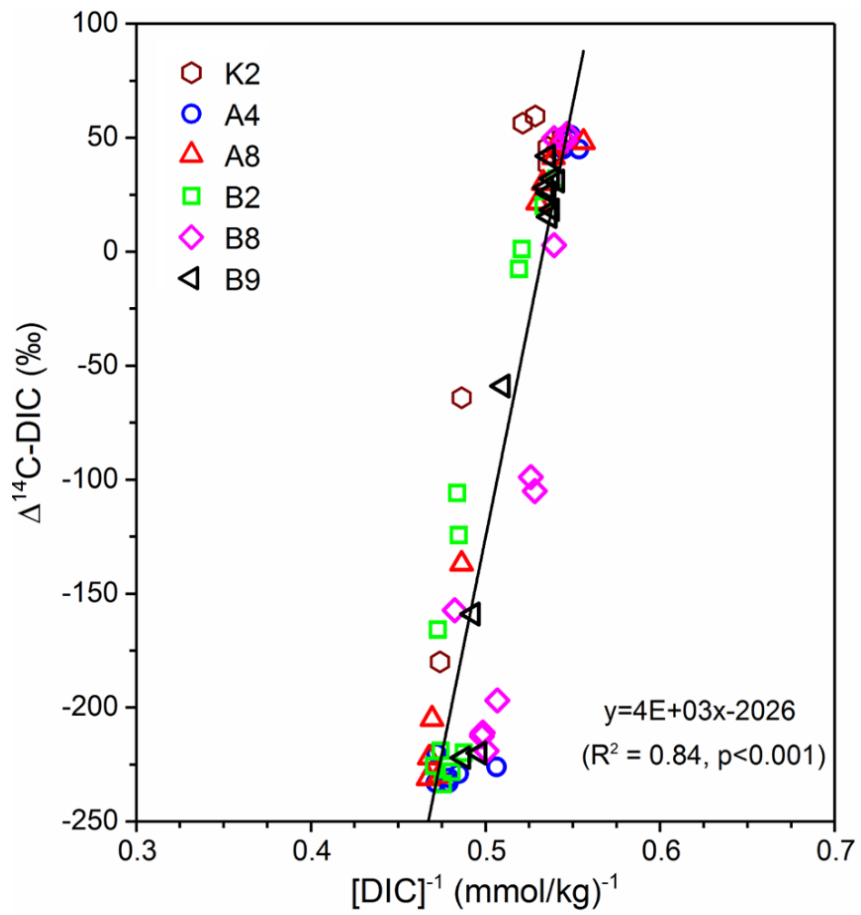
776



777

778 **Figure 9.** Transectional distributions of (a) salinity, (b) DOC concentrations, (c) DIC
 779 concentration and (d) $\Delta^{14}\text{C-DIC}$ values for (e) stations (black squares) sampled across the
 780 Kuroshio Extension (KE) in the northwestern North Pacific. Black dots indicate depths where
 781 samples were collected. Note: (a) The salinity of another five stations (yellow circles) along the
 782 35°N transect are included to support the spreading of the data. The hydrographic data for the
 783 five reference stations are taken from the Pacific data source in <https://www.nodc.noaa.gov/ocads/>. (c-d) DIC concentrations and $\Delta^{14}\text{C-DIC}$ values are given only for four stations due to
 784 the lack of data at Sta. A1-b (Ding et al., 2018).
 785

786



787

788 **Figure 10.** Keeling plot of $\Delta^{14}\text{C-DIC}$ vs. concentration of $[\text{DIC}]^{-1}$ measured for six stations (B9,
 789 B8, A4, A8, B2 and K2) in the northwestern North Pacific (data from Ding et al. (2018)). The
 790 line indicates the linear regression fit to all data points.

791